Journal of Magnetism and Magnetic Materials 320 (2008) 2746–2751

Contents lists available at ScienceDirect

Journal of Magnetism and Magnetic Materials

journal homepage: www.elsevier.com/locate/jmmm

Structural and magnetic properties of $SrFe_{12}O_{19}$ hexaferrite synthesized by a modified chemical co-precipitation method

Z.F. Zi [a,b,c], Y.P. Sun [a,b,*], X.B. Zhu [a,b], Z.R. Yang [a,b], J.M. dai [a,b], W.H. Song [a,b]

[a] Key Laboratory of Materials Physics, Institute of Solid State Physics, Hefei 230031, PR China
[b] Hefei High Magnetic Field Laboratory, Chinese Academy of Sciences, Hefei 230031, PR China
[c] Department of Physics and Electronic Engineering, Hefei Teachers College, Hefei 230061, PR China

ARTICLE INFO

Article history:
Received 21 March 2008
Received in revised form
26 May 2008
Available online 12 June 2008

PACS:
75.50.Gg
75.50.Tt
76.50.+g
81.20.Fw

Keywords:
Strontium hexaferrite
Chemical co-precipitation method
Coercivity
Multi-domain

ABSTRACT

M-type strontium hexaferrite ($SrFe_{12}O_{19}$) particles had been prepared by a modified chemical co-precipitation route. Structural and magnetic properties were systematically investigated. Rietveld refinement of X-ray powder diffraction results showed that the sample was single-phase with the space group of $P6_3/mmc$ and cell parameter values of $a = 5.8751$ Å and $c = 23.0395$ Å. The results of field-emission scanning electronic microscopy showed that the grains were regular hexagonal platelets with sizes from 2 to 4 μm. The composition determined by energy dispersive spectroscopy is the stoichiometry of $SrFe_{12}O_{19}$. The ferrimagnetic to paramagnetic transition was sharp with Curie temperature $T_C = 737$ K, which further confirmed that the samples were single phase. However, it was found that the coercivity, saturation magnetization and the squareness ratio of the synthesized $SrFe_{12}O_{19}$ samples were lower than the theoretical values, which could be explained by the multi-domain structure and the increase of the demagnetizing factor.

1. Introduction

M-type strontium hexaferrite ($SrFe_{12}O_{19}$) was discovered in the 1950s by Philips' laboratories [1]. Due to appropriate magnetic properties, chemical stability, and low cost compared with rare-earth compounds, it has attracted extensive interests in the past decades [2–4]. It is a hard magnet with high coercivity, which originates from high magnetocrystalline anisotropy with single easy magnetization axis. It has been recognized that it can be used as permanent magnets, recording media, telecommunication, and as components in microwave, higher-frequency, and magneto-optical devices [5–11].

The structure of *M*-type hexagonal is stacked alternatively by spinel ($S = Fe_6O_8^{2+}$) and hexagonal ($R = MFe_6O_{11}^{2-}$) layers. The O^{2-} ions exist as close-packed layers, with the M^{2+} substituting for an O^{2-} in the hexagonal layer. The Fe^{3+} ions are distributed in the five interstitial crystallographic sites of the close-packed layers, i.e. three octahedral (2a, 12k and $4f_2$), one tetrahedral ($4f_1$), and one trigonal bipyramid (2b). The three parallel (2a, 12k and 2b) and two antiparallel ($4f_1$ and $4f_2$) sub-lattices, which are coupled by superexchange interactions through the O^{2-} ions, form the ferrimagnetic structure [12–14]. A schematic *M*-type structural representation and the surroundings of five Fe^{3+} sites are shown in Fig. 1 by Collomb et al. [15].

Because the magnetic properties of $SrFe_{12}O_{19}$ strongly depend on the size and shape of the particles [16,17], several routes have been used to prepare strontium ferrite, including the traditional sol–gel process [18,19], the solid-state method [17,20], the salt-melting method [21], ball milling [22,23], self-propagating high-temperature synthesis [24], and the chemical co-precipitation method [25].

As it is well known, the chemical co-precipitation method is usually used to synthesize magnetic oxides due to its simplicity and good-control of grain size. However, in previous reports it was always observed that there exist some undesirable intermediate non-ferromagnetic phases, which lead to poor magnetic properties and irregular shape for the derived $SrFe_{12}O_{19}$ particles [26]. In this paper, single-phase $SrFe_{12}O_{19}$ particles with relatively homogeneous size are successfully prepared by means of a modified chemical co-precipitation method. In the processing, ammonium oxalate monohydrate was used as a precipitator instead of alkali in order to control effectively the nucleation and growth of $SrFe_{12}O_{19}$ particles. As a result, the grain size, shape and size distribution are well controlled.

* Corresponding author at: Key Laboratory of Materials Physics, Institute of Solid State Physics, Hefei 230031, PR China. Fax: +86 0551 5591434.
E-mail addresses: zizhenfa@126.com (Z.F. Zi), ypsun@issp.ac.cn (Y.P. Sun).

0304-8853/$ - see front matter © 2008 Elsevier B.V. All rights reserved.
doi:10.1016/j.jmmm.2008.06.009

2. Experimental

Micron-sized $SrFe_{12}O_{19}$ particles were prepared by the chemical co-precipitation method. All starting precursors were of high-purity compounds. First, $Sr(NO_3)_2$ and $Fe(NO_3)_3 \cdot 9H_2O$ with Sr:Fe atomic ratio of 1:12 were dissolved in deionized water by gentle heating. Then, the aqueous mixture was slowly poured into $(NH_4)_2C_2O_4 \cdot H_2O$ solution and stirred for several minutes using a magnetic stirrer. The gelatinous precipitate was filtered and washed several times using deionized water until the pH value of the solution became neutral. The dried powders were sintered at 500 °C for 8 h in air, and then sintered at 1100 °C for 8 h in air. Finally, the obtained powders were pressed into pellets with Φ $10 \times 2\,mm^2$ under a pressure of 20 MPa and sintered at 1000 °C for 10 h in air.

The crystal structure was examined by Philips X'pert PRO X-ray diffractometer (XRD) with CuK_α radiation at room temperature. The morphology of grains was investigated by field-emission scanning electronic microscopy (FE-SEM), and the compositions were examined by the energy dispersive spectroscopy (EDS) in FE-SEM. Magnetization measurements from room temperature to 800 K were performed using a vibrating-sample magnetometer (VSM) accompanied by a quantum design physical properties measurement system (PPMS) ($1.8\,K \leqslant T \leqslant 1000\,K$, $0\,T \leqslant H \leqslant 9\,T$).

3. Results and discussion

The room-temperature powder XRD pattern and Rietveld refinement of $SrFe_{12}O_{19}$ sample are shown in Fig. 1. The good

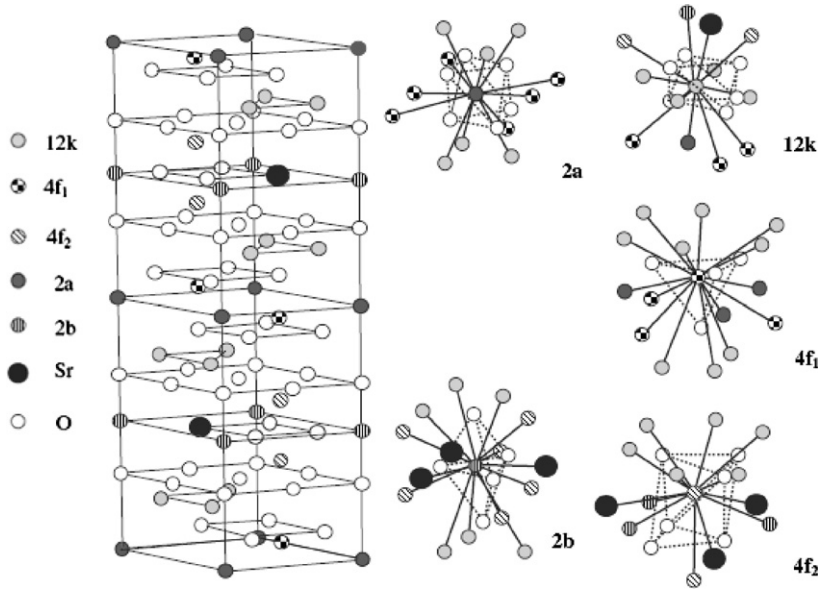

Fig. 1. The crystal structure sketch map of the hexagonal *M*-type phase and the five Fe sites with their surroundings are displayed, which is taken from Ref. [15].

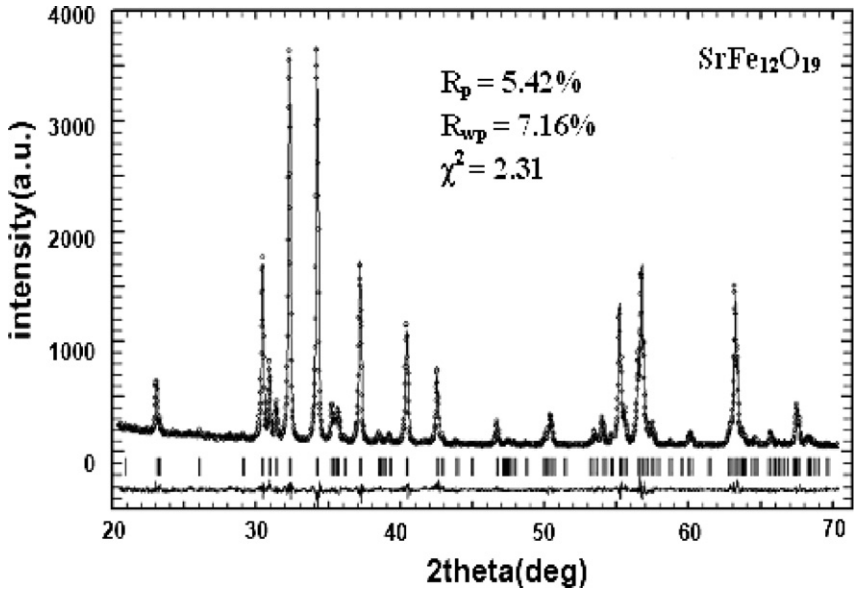

Fig. 2. The output from the Rietveld refinement analysis of the XRD pattern for $SrFe_{12}O_{19}$ sample. The plus signs show raw experimental data, and the continuous line overlapping them refers to the calculated data. The vertical bars are the expected Bragg reflection positions. The difference between the experimental data and the calculated data is shown at the bottom.

fitting parameters, $R_p = 5.42\%$, $R_{wp} = 7.16\%$, $\chi^2 = 3.71$, suggest that the derived samples are of high quality (Fig. 2). All of peaks can be successfully indexed to hexagonal magnetoplumbite structure with a space group of $P6_3/mmc$. The refined lattice parameter values are of $a = b = 5.8751$ Å and $c = 23.0395$ Å. The above values are well in accord with the previous reports for $SrFe_{12}O_{19}$ [17]. The refined atomic positions for the $SrFe_{12}O_{19}$ sample are shown in Table 1. In Rietveld analysis, the refined parameters were scale factor, background parameters, 2θ zero-point, lattice constants, profile half-width parameters (u, v, w), the mixing parameters of the Pseudo-Voigt function (N_A, N_B), asymmetry correction factor (P), occupancy, atomic functional positions, and isotropic thermal parameters. The structure, profiles, and important bond lengths (Å) and angles (deg) calculated for $SrFe_{12}O_{19}$ are listed in Table 2.

FE-SEM images are shown in Fig. 3. It is clearly seen that the grains are regular hexagonal platelets with rather homogenous grain sizes from 2 to 4 μm. A quantitative EDS analysis is used to determine the composition, and the result is shown in Fig. 4. The results show that the molar ratio of Sr, Fe and O is about 1:11.86:19.11, which is almost consistent with the nominal composition, suggesting that the obtained sample is near stoichiometric. A small quantity of C element may come from electrically conductive glue on the specimen holder.

Fig. 5 is the diameter distribution of the $SrFe_{12}O_{19}$ particles, which shows that the average diameter of the obtained $SrFe_{12}O_{19}$ particles is about 3 μm. This sample has a narrow grain size distribution and the diameters of most $SrFe_{12}O_{19}$ particles are estimated to be between 2 and 4 μm.

To investigate the magnetic properties of the synthesized $SrFe_{12}O_{19}$ sample, the temperature dependence of magnetization $M(T)$ and the applied magnetic field dependence of magnetization $M(H)$, i.e. the magnetic hysteresis loop, are measured. The measured $M(T)$ curve of the $SrFe_{12}O_{19}$ sample under field cooling (FC) modes with measuring field $H = 100$ Oe is shown in Fig. 6. It can be seen that $SrFe_{12}O_{19}$ sample shows a sharp ferrimagnetic to paramagnetic transition, and the Curie temperature T_C derived by the peak of $dM(T)/dT$ as shown in the inset of Fig. 6 is 737 K, which is slightly lower than those reported in Refs. [2,27].

The $M(H)$ loop for the $SrFe_{12}O_{19}$ sample at 300 K is shown in Fig. 7. It is clear that the value of saturation magnetization (M_s) comes out to be 55.73 emu/g at room temperature, which is smaller than the theoretically predicted value (67.70 emu/g), but agrees well with other experimental values by different preparation methods [16]. The remanence magnitude M_r can be extracted from the hysteresis loop at the intersections of the loop with the vertical magnetization axis. The M_r value of 16.23 emu/g of the $SrFe_{12}O_{19}$ sample is obtained from Fig. 7.

The squareness ratio (SQR) of the $SrFe_{12}O_{19}$ sample is denoted by the ratio M_r/M_s. The value is essentially a measure of squareness of the hysteresis loop. In general, large SQR value is preferred in many applications such as magnetic recording media

Table 1
Atomic positions obtained from Rietveld refinement for the $SrFe_{12}O_{19}$ sample

Atom	Site	x	y	z
Sr	2d	0.6667	0.3333	0.2500
Fe1	2a	0.0000	0.0000	0.0000
Fe2	2b	0.0000	0.0000	0.2558
Fe3	4f1	0.3333	0.6667	0.0271
Fe4	4f2	0.3333	0.6667	0.8997
Fe5	12k	0.1692	0.3388	0.8906
O1	4e	0.0000	0.0000	0.1489
O2	4f	0.3333	0.6667	0.9436
O3	6h	0.1784	0.3761	0.2500
O4	12k	0.1576	0.3158	0.0527
O5	12k	0.5053	0.0110	0.1523

Table 2
Bond lengths, bond angles, and lattice constants from Rietveld refinement for the $SrFe_{12}O_{19}$ sample

Type	Bond length/ (Å)	Type	Bond length/ (Å)	Type	Bond angle/ (deg)
Sr–O	2.8601	Fe4–O5	1.8916	Fe2–O1–Fe5	117.91
Sr–Fe2	3.3958	Fe5–O1	2.0674	Fe3–O2–Fe5	126.22
Sr–Fe5	3.6478	Fe5–O2	1.9511	Fe5–O1–Fe5	99.90
Fe1–O4	2.0058	Fe5–O4	2.1241	Fe5–O4–Fe5	89.34
Fe2–O1	2.4583	Fe5–O5	1.9336		
Fe2–O3	1.8904	Fe2–Fe4	3.6661		
Fe3–O2	1.9171	Fe2–Fe5	3.7123	Lattice constant	
Fe3–O4	1.8792	Fe4–Fe4	2.7672	$a = 5.8751$ Å	
Fe4–O3	2.0302	Fe5–Fe5	2.9860	$c = 23.0395$ Å	

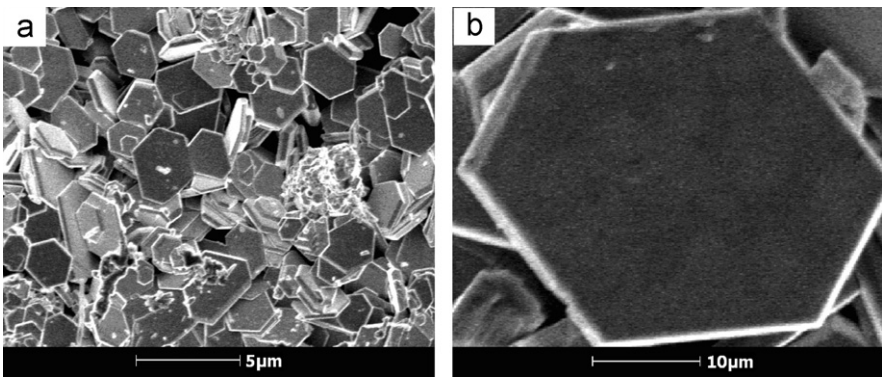

Fig. 3. Typical FE-SEM images of $SrFe_{12}O_{19}$ particles synthesized by the chemical co-precipitation method.

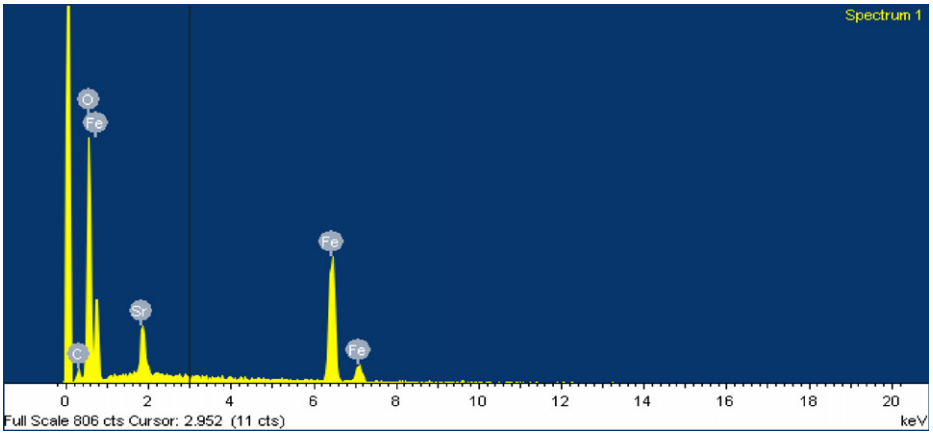

Fig. 4. EDS analysis image of the $SrFe_{12}O_{19}$ particles.

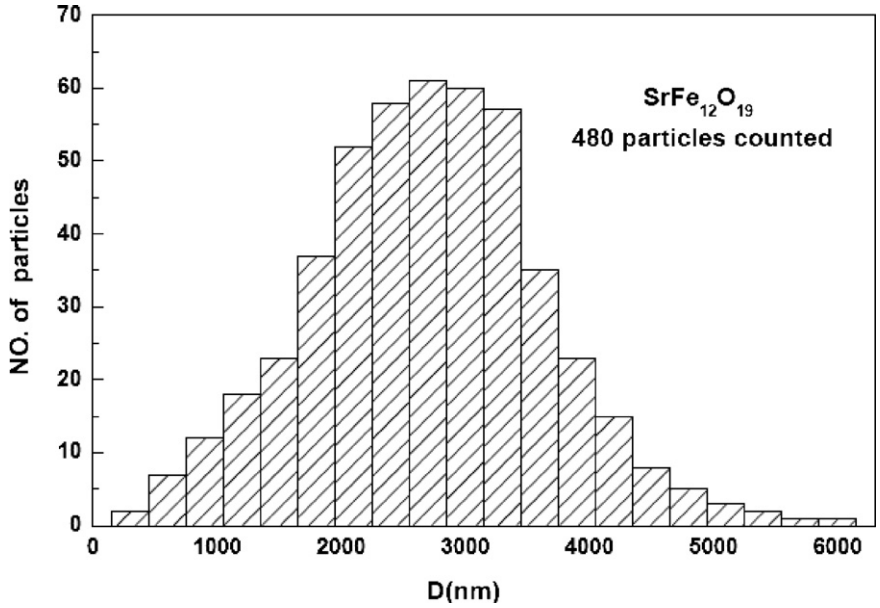

Fig. 5. Particle size distribution of $SrFe_{12}O_{19}$ particles synthesized by the co-precipitation method.

of high density and permanent magnets. The SQR of our $SrFe_{12}O_{19}$ sample is calculated as 0.29.

The coercivity for a ferromagnet or ferrimagnet can be reflected by coercivity field H_c. The value refers to the intensity of the magnetic field required to reduce the magnetization of the magnetic sample to zero, after the magnetization of the sample has reached saturation. The obtained value of H_c (1.06 kOe) for our sample is much lower than those of the literature and the theoretical limit (7.5 kOe) [16,28]. There are two following possible reasons. On the one hand, the grain size of the $SrFe_{12}O_{19}$ particles in this study was between about 2 and 4 μm. The critical size of a single-domain particle is estimated using the formula [29]

$$D_m = 9\sigma_w/2\pi M_s^2$$

where $\sigma_w = (2k_BT_C|K_1|/a)^{1/2}$ is the wall density energy, $|K_1|$ is the magnetocrystalline anisotropy constant, T_C is the Curie temperature, M_s is the saturation magnetization, k_B is the Boltzmann constant and a is the lattice constant. For $D > D_m$ the particles are multi-domain structures, while for $D < D_m$ the particles are mono-domain structures. For $SrFe_{12}O_{19}$, $T_C = 737$ K, $a = 6 \times 10^{-8}$ cm, $|K_1| = 3.7 \times 10^6$ erg/cm^3 and $M_s = 280$ Gs, the value of D_m estimated is about 650 nm, which is far smaller than the average diameter of the obtained $SrFe_{12}O_{19}$ particles. So the grains exhibit a multi-domain behavior. The formation of multi-domain and the easy movement of the domain walls result in the decrease of the coercivity. On the other hand, in M-type strontium hexaferrite, the magnetic easy axis lies within the basal plane. The demagnetizing factor in a disk shape for a $SrFe_{12}O_{19}$ particle increases with the increase of width to thickness ratio, which leads to a decrease in the coercivity [30]. Consequently, the regular hexagonal plate-like morphology as shown in Fig. 3 leads to lower coercivity than the theoretical prediction.

The coercivity (H_c), saturation magnetization (M_s), and the SQR of the $SrFe_{12}O_{19}$ sample are closely correlated not only to the grain size but also to the method of preparation. It is possible to obtain higherquality samples with desirable H_c, M_s, and SQR by optimizing the processing parameters.

4. Conclusions

A modified chemical co-precipitation method was used to prepare M-type $SrFe_{12}O_{19}$ hexaferrite. The XRD result showed that

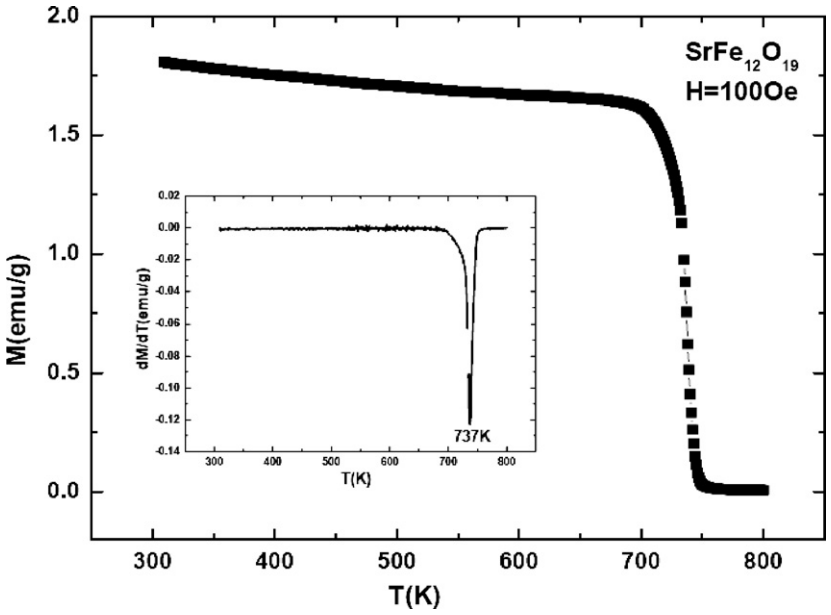

Fig. 6. Magnetization versus temperature curve for the $SrFe_{12}O_{19}$ sample. The inset is the temperature dependence of the first derivative of $M(T)$, $dM(T)/dT$.

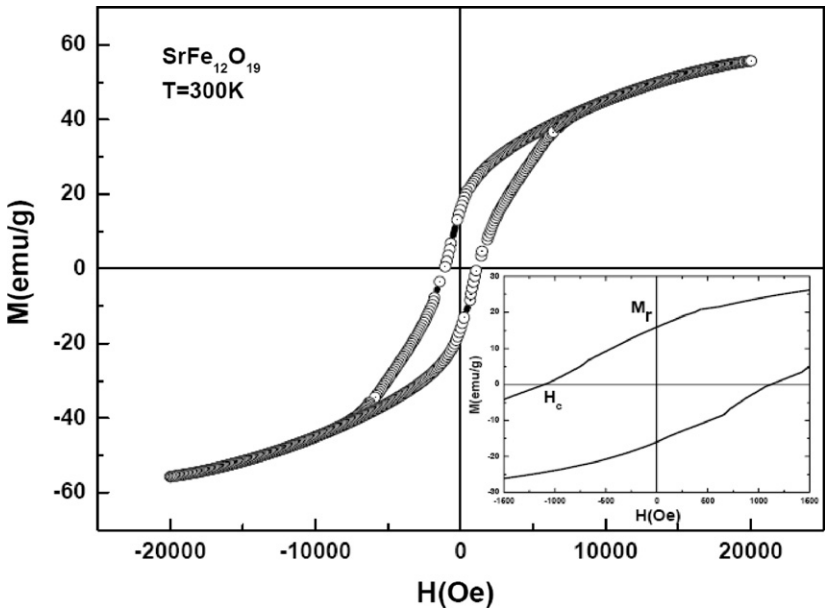

Fig. 7. Room-temperature M–H hysteresis loop of $SrFe_{12}O_{19}$ sample. The inset contains the minor loop.

the derived sample was pure phase with $P6_3/mmc$. FE-SEM results showed that the grains were regular hexagonal platelets with sizes from 2 to 4 μm. The magnetic properties including Curie temperature, room temperature M_s, M_r, SQR, and H_c were investigated. The reduction of magnetic properties could be explained by the multi-domain structure and the increase of demagnetizing factor.

Acknowledgments

This work was financially supported by the National Key Basic Research Program of China under contract No. 2007CB925002 and the National Nature Science Foundation of China under contract No.10774146, 10774147, 50672099, 50701042 and Director's Fund of Hefei Institutes of Physical Science, Chinese Academy of Sciences.

References

[1] J.J. Went, G.W. Ratheneau, E.W. Gorter, G.W. VanDosterhout, Philips Tech. Rev. 13 (1951) 194.
[2] B.T. Shirk, W.R. Buessem, J. Appl. Phys. 40 (1969) 1294.
[3] J.G. Rensen, J.S. van Wieringen, Solid State Commun. 7 (1969) 1139.
[4] E. Kreber, U. Gonser, A. Trautwein, F.E. Harris, J. Phys. Chem. Solids 36 (1975) 263.
[5] J.M.D. Coey, J. Alloys Compd. 326 (2001) 2.
[6] P.E. Kazin, L.A. Trusov, D.D. Zaitsev, Yu.D. Tretyakov, M. Jansen, J. Magn. Magn. Mater. 320 (2008) 1068.
[7] A. Morisako, T. Naka, K. Ito, A. Takizawa, M. Matsumoto, K.Y. Hong, J. Magn. Magn. Mater. 242 (2002) 304.
[8] P. Hernandez, C.D. Francisco, J.M. Munoz, J. Iniguez, L. Torres, M. Zazo, J. Magn. Magn. Mater. 157 (1996) 123.

[9] Z. Jin, W. Tang, J. Zhang, H. Lin, Y. Du, J. Magn. Magn. Mater. 182 (1998) 231.
[10] Muhammad Javed Iqbal, Muhammad Naeem Ashiq, Pablo Hernandez-Gomez, Jose Maria Munoz, J. Magn. Magn. Mater. 320 (2008) 881.
[11] B.T. Shirk, W.R. Buessem, J. Am. Ceram. Soc. 53 (1970) 192.
[12] L. Lechevallier, J.M.L. Breton, J.F. Wang, I.R. Harris, J. Magn. Magn. Mater. 269 (2004) 192.
[13] M. Pieper, A. Morel, F. Kools, J. Magn. Magn. Mater. 242 (2002) 1408.
[14] A. Morel, J.M. Le Breton, J. Kreisel, G. Wiesinger, F. Kools, P. Tenaud, J. Magn. Magn. Mater. 242 (2002) 1405.
[15] A. Collomb, B. Lambert Andron, J.X. Boucherle, D. Samaras, Phys. Stat. sol. (A) 96 (1986) 385.
[16] A. Ataie, S. Heshmati Manesh, J. Eur. Ceram. Soc. 21 (2001) 1951.
[17] D.H. Chen, Y.Y. Chen, Mater. Res. Bull. 37 (2002) 801.
[18] P.C.A. Brito, R.F. Gomes, J.G.S. Duqueb, M.A. Mace do, Physica B 384 (2006) 91.
[19] Ali Ghasemi, Akimitsu Morisako, J. Magn. Magn. Mater. 320 (2008) 1167.
[20] H. How, X. Zuo, C.V. Wave, IEEE Trans. Magn. 41 (2005) 2349.
[21] Z.B. Guo, W.P. Ding, W. Zhong, J.R. Zang, Y.W. Do, J. Magn. Magn. Mater. 175 (1997) 333.
[22] W.A. Kaczmarek, B. Idzikowski, K.H. Muller, J. Magn. Magn. Mater. 177 (1998) 921.
[23] S.V. Ketov, Yu.D. Yagodkin, A.L. Lebed, Yu.V. Chernopyatova, K. Khlopkov, J. Magn. Magn. Mater. 300 (2006) e479.
[24] L. Qiao, L.H. You, J.W. Zheng, L.Q. Jiang, J.W. Sheng, J. Magn. Magn. Mater. 318 (2007) 74.
[25] V.V. Pankov, M. Pernet, P. Germi, P. Mollard, J. Magn. Magn. Mater. 120 (1993) 69.
[26] M.M. Hessien, M.M. Rashad, K. El-Barawy, J. Magn. Magn. Mater. 320 (2008) 336.
[27] Balwinder Kaur, Monita Bhat, F. Licci, Ravi Kumar, S.D. Kulkarni, P.A. Joy, K.K. Bamzai, P.N. Kotru, J. Magn. Magn. Mater. 305 (2006) 392.
[28] X.H. Wang, L. Li, Z. Gui, S. Shu, J. Zhou, Mater. Chem. Phys. 77 (2002) 248.
[29] J. Smit, H.P.J. Wijn, Les Ferrites, Dunod, Paris, 1961.
[30] E.C. Stoner, E.P. Wohlfarth, Philos. Trans. R. Soc. London A 240 (1948) 599.